

Article

Enhanced Photocatalytic Activity of TiO₂ Thin Film Deposited by Reactive RF Sputtering under Oxygen-Rich Conditions

Takaya Ogawa , Yuekai Zhao, Hideyuki Okumura and Keiichi N. Ishihara 

Graduate School of Energy Science, Kyoto University, Kyoto 606-8501, Japan; yuekai1994@163.com (Y.Z.); okumura.hideyuki.4e@kyoto-u.ac.jp (H.O.); ishihara.keiichi.6w@kyoto-u.ac.jp (K.N.I.)

* Correspondence: ogawa.takaya.8s@kyoto-u.ac.jp

Abstract: TiO₂ thin films are promising as photocatalysts to decompose organic compounds. In this study, TiO₂ thin films were deposited by reactive radio-frequency (RF) magnetron sputtering under various flow rates of oxygen and argon gas. The results show that the photocatalytic activity decreases as the oxygen-gas ratio is increased to 30% or less, while the activity increases under oxygen-rich conditions. It was observed that the crystal structure changed from anatase to a composite of anatase and rutile, where the oxygen-gas ratio during RF sputtering is more than 40%. Interestingly, the oxygen vacancy concentration increased under oxygen-rich conditions, where the oxygen-gas ratio is more than 40%. The sample prepared under the most enriched oxygen condition, 70%, among our experiments exhibited the highest concentration of oxygen vacancy and the highest photocatalytic activity. Both the oxygen vacancies and the composite of anatase and rutile structure in the TiO₂ films deposited under oxygen-rich conditions are considered responsible for the enhanced photocatalysis.

Keywords: TiO₂ thin film; photocatalyst; oxygen and argon gas flow rates



Citation: Ogawa, T.; Zhao, Y.; Okumura, H.; Ishihara, K.N.

Enhanced Photocatalytic Activity of TiO₂ Thin Film Deposited by Reactive RF Sputtering under Oxygen-Rich Conditions. *Photochem* **2022**, *2*, 138–149. <https://doi.org/10.3390/photochem2010011>

Academic Editor: Vincenzo Vaiano

Received: 15 January 2022

Accepted: 11 February 2022

Published: 18 February 2022

Publisher's Note: MDPI stays neutral with regard to jurisdictional claims in published maps and institutional affiliations.



Copyright: © 2022 by the authors. Licensee MDPI, Basel, Switzerland. This article is an open access article distributed under the terms and conditions of the Creative Commons Attribution (CC BY) license (<https://creativecommons.org/licenses/by/4.0/>).

1. Introduction

Thin films of photocatalysts have been intensively studied as clean technology [1–3]. Photocatalytic thin films can decompose various organic compounds in a solution using energy from sunlight, and it is relatively easy to separate the catalysts from the solution. Among many photocatalysts, TiO₂ is promising due to its low cost, stable availability, high durability, and less risk to the human body and environment [4–7]. There are three major TiO₂ crystalline forms: anatase, rutile, and brookite. The rutile phase is the most stable in bulk at room temperature and ambient pressure.

Several techniques can be used to deposit TiO₂ thin films [8], such as the sol-gel method [3,9], spray pyrolysis [10], pulsed laser deposition [11], e-beam evaporation [12], chemical vapor deposition [13], and sputtering [14]. Notably, reactive radio-frequency (RF) magnetron sputtering is a promising technique with desirable features such as excellent film adhesion and uniform distribution of thickness [15]. It is possible to form films with various electronic states and microstructures via changing sputtering conditions, such as RF power, deposition pressure, substrate temperature, and gas flow rate. Especially, it is the characteristic of reactive sputtering that can control oxygen contents. Then, the oxygen gas ratio (R_{O_2} : $[O_2 \text{ gas flow rate}]/[(Ar + O_2) \text{ gas flow rate}]$) is one of the most critical parameters for photocatalytic activity [16], although the effect of the R_{O_2} is still controversial. Zhang et al. reported that TiO₂ film deposited under a high argon flow rate absorbs more light irradiation, which results in more electron–hole pairs generated in the TiO₂ film and thus enhanced photocatalytic activity [17]. Huang et al. and Chiou et al. demonstrated that the photocatalytic activity of TiO₂ films is raised with increasing oxygen flow rate to some extent but finally dropped at the high values of R_{O_2} [18,19]. Furthermore, the wide range of R_{O_2} conditions was not tested without heating substrate (see Table S1 in Supporting Information).

In this study, we synthesized TiO₂ thin films via reactive RF sputtering at the condition with the R_{O2} values ranging from 0 to 70%. In this study, we synthesized TiO₂ thin films via reactive RF sputtering with changing R_{O2} and examined the parameters that influence photocatalytic activity. As the R_{O2} was increased, the photocatalytic activity decreased with the R_{O2} values up to 30% and increased with the R_{O2} values over 40%. We investigated the oxygen vacancy concentration, and it decreased with the R_{O2} values up to 30–40%, which is a general behavior under the oxygen-rich conditions [15,20]. On the other hand, interestingly, the vacancy concentration was increased with the R_{O2} values of more than 40%. In addition, other film properties also showed a change in their tendency at around R_{O2} = 40%. These are considered to involve enhanced photocatalytic activity to decompose an organic dye. A possible explanation of the phenomena will be provided to suggest suitable deposition conditions for highly active thin-film photocatalysts.

2. Experimental Details

2.1. Synthesis of TiO₂ Thin Films

TiO₂ thin films were deposited on a glass slide substrate using a reactive RF magnetron sputtering method with pure titanium (Ti) target. The deposition was performed without a substrate heater, while the temperature should be slightly raised by the sputtering energy. The distance between the substrate and the target was 70 mm. The glass slide substrates with the size of 24 × 48 × 1.2 mm were purchased from Toshinriko Co. Ltd (Tokyo, Japan). The sputtering equipment is RSC-MG2 produced by CryoVac Inc. (Osaka, Japan). The target is 99.9% pure titanium provided from Kojundo Chemical Laboratory Co., Ltd., (Sakado, Japan). Before deposition, pre-sputtering with a sputtering power of 300 W was conducted to clean the surface of the Ti target under Ar gas (100 sccm). The deposition time for a sample was 2 h with a sputtering power of 300 W. During the sputtering, the total flow rate of Ar and O₂ gases was 100 sccm under a pressure of 4.0 × 10⁻³ Pa. Eight samples were prepared with different ratios of O₂ gas (R_{O2}: [O₂ gas flow rate]/[(Ar + O₂) gas flow rate]) = 5%, 10%, 20%, 30%, 40%, 50%, 60%, and 70%). The following characterization methods were conducted on these samples as deposited.

2.2. Characterization

The crystalline structures were characterized by X-ray diffractometry (XRD) (RINT2100CMJ, produced by Rigaku Co., Ltd., Tokyo, Japan) using Cu K α radiation (λ = 1.54184 Å), operated at 40 kV and 30 mA.

The transmittance measurements of thin-film samples were performed using UV-vis spectroscopy (Lambda750S produced by PerkinElmer Co., Ltd., Waltham, MA, USA) in the wavelength range between 250 nm and 800 nm. The average transparency was determined in the visible light range from 380 nm to 740 nm. The band gaps of thin film samples were estimated using the Tauc plot method. The TiO₂ was reported to have both a direct forbidden and an indirect allowed transition, where the latter transition dominates the optical absorption due to the weak strength of the former transition. Thus, we assumed only the indirect allowed transitions.

A field emission scanning electron microscope (FE-SEM, SU6600 produced by Hitachi High-Technologies Co., Ltd., Tokyo, Japan) was used to observe the surface morphology of the thin-film samples at an accelerating voltage of 20.0 kV. The average diameter was estimated via ImageJ.

The chemical composition and chemical bonding states of TiO₂ thin films were investigated by X-ray photoelectron spectroscopy (XPS) analysis (JPS-9030 produced by JEOL Co., Ltd., Tokyo, Japan), operated at 10.0 kV and 20.0 mA. A standard MgK α X-ray source was employed, and the measurement area had a diameter of 10 mm. A high-etching-rate ion gun with Ar ions was employed to remove the contaminants and hydroxyl (OH) groups on the specimen surface. The approximate etched depth was 0.2 nm. The obtained data were analyzed using the software SPECSURF Analysis, which is built-in for JEOL XPS. The Ti³⁺ and Ti⁴⁺ peak areas were utilized to estimate oxygen vacancy concentrations (Ti³⁺ ratio:

$[\text{Ti}^{3+} \text{ peak area}]/[(\text{Ti}^{3+} + \text{Ti}^{4+}) \text{ peak area}]$ because one Ti^{3+} ion in TiO_2 requires one oxygen vacancy to accommodate charge neutrality [21].

2.3. Measurement of Photocatalytic Activity

The photocatalytic activity was evaluated via the decomposition rate of methyl orange (MO). The MO granular solid (purity: 99.9%; produced by Nacalai Tesque Inc., Kyoto, Japan) was used to prepare a MO solution with a concentration of 0.01 mmol/L, and 16 mL was utilized for photocatalytic measurements.

A xenon lamp (UXL-500D-O produced by Ushio Co., Ltd., Tokyo, Japan) located above the solution was used as the light source, which included both ultraviolet light and visible light (the spectra of the lamp were shown in Figure S1 in Supporting Information). The power of the lamp was 500 W. A tube with 15 cm (height) of water was placed between the Xenon lamp and the MO solution to filter the infrared light of the Xenon lamp irradiation and maintain the temperature. During the photoactivity measurement, the solution was stirred at 1200 rpm, and the concentration changes in MO were monitored every 20 min via spectrophotometry.

3. Results

3.1. XRD Measurements

Figure 1 shows XRD patterns of the TiO_2 thin films deposited under various oxygen flow rates. The patterns indicate that the anatase structure is dominant except for $R_{\text{O}_2} = 70\%$. As the R_{O_2} value increases (from 5%), the diffraction peak corresponding to the (110) plane of the rutile phase at around $2\theta = 27^\circ$ was not prominent until $R_{\text{O}_2} = 30\text{--}40\%$. However, at R_{O_2} greater than 40%, the rutile structure was distinguished and became comparable with the anatase structure at $R_{\text{O}_2} = 70\%$. The crystallite sizes of the films estimated via Scherrer's equation are shown in Table S1 in the Supporting Information. The crystallite sizes did not indicate the correlation with R_{O_2} .

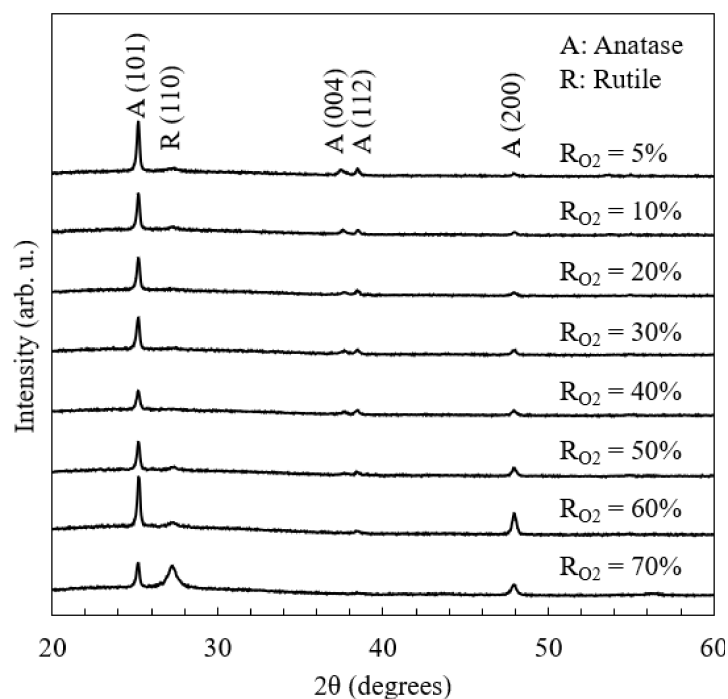


Figure 1. XRD patterns of TiO_2 thin films.

3.2. Optical Transmittance Spectra

Figures 2–4 show the optical transmittance spectra of TiO_2 thin films, an example of a Tauc plot based on the spectra, and the band gaps based on Tauc plots, respectively. As the R_{O_2} value was increased, the band gap was also increased until $R_{\text{O}_2} = 20\%$, remained

constant until 30–40%, and decreased over $R_{O_2} = 40\%$. The reported band gaps of the anatase and rutile structures are 3.2 eV and 3.0 eV, respectively, for bulk TiO_2 [22]. The constant value, around 3.32 eV, at $R_{O_2} = 20\text{--}40\%$ could be derived from the anatase structure, where the difference of 0.12 eV larger than 3.2 eV is explained by the tendency that the band gap of thin films is generally wider than that of bulk [23,24]. The relatively smaller values of band gap at $R_{O_2} = 5\text{--}10\%$ should originate from the rutile structure, which was slightly detected in XRD results. The rutile structure has a narrower band gap than the anatase structure. The narrower band gaps in the other R_{O_2} region should be due to the composite of the rutile and the anatase structure, which is consistent with XRD results. In fact, the rutile structure mostly disappeared in XRD patterns at $R_{O_2} = 20\text{--}40\%$. Therefore, the change in the band gap is mainly attributed to the crystal structure, though the film strain could modify the band gap value.

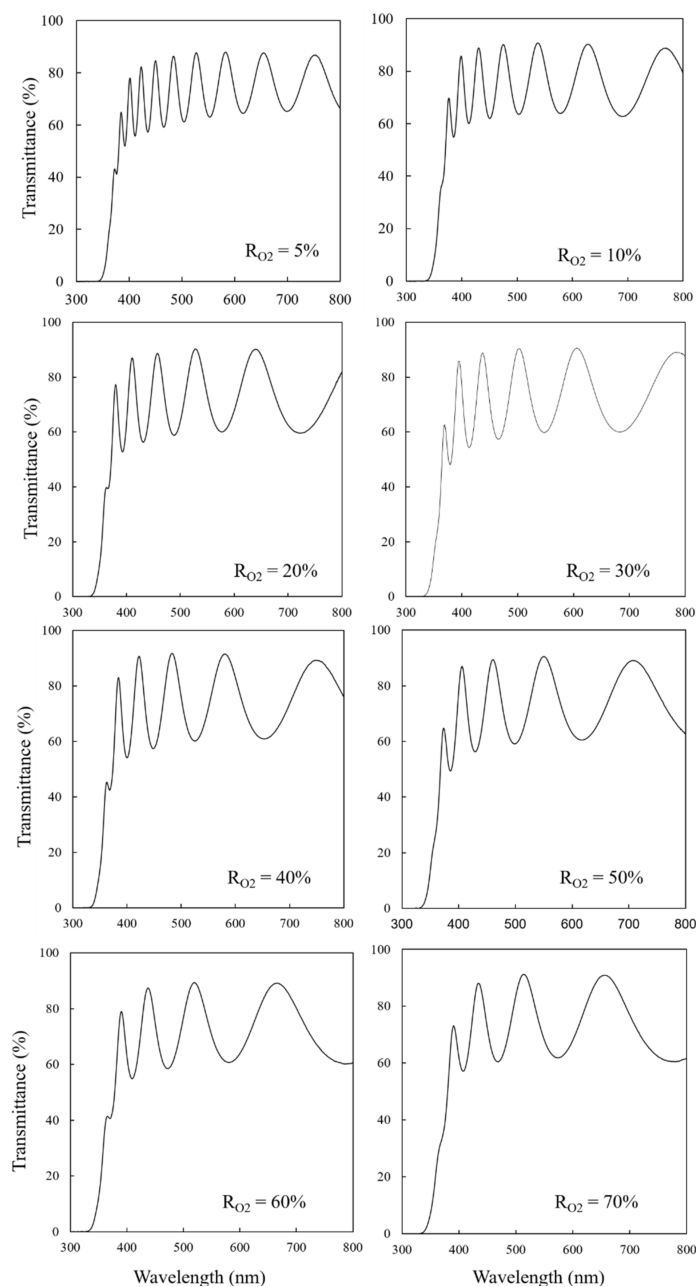


Figure 2. Optical transmittance spectra of TiO_2 thin films.

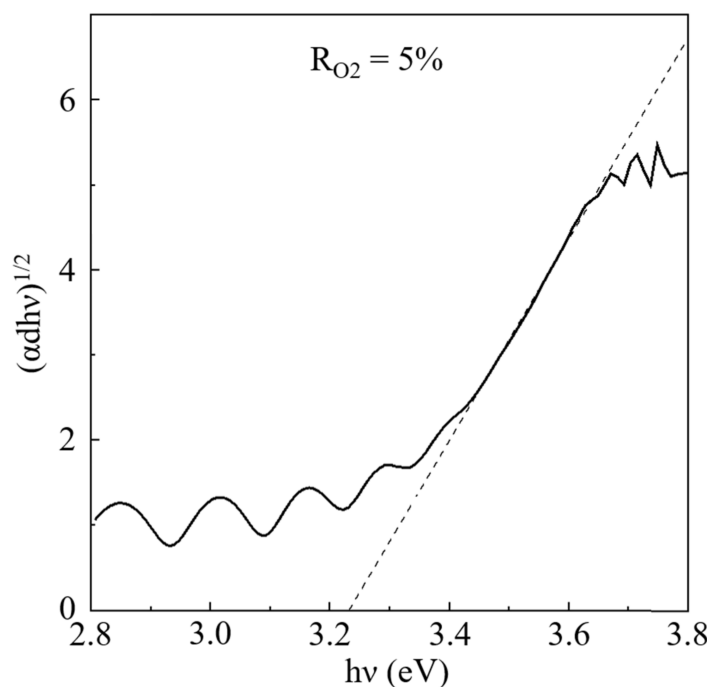


Figure 3. An example of Tauc plot (the sample deposited under $R_{O_2} = 5\%$).

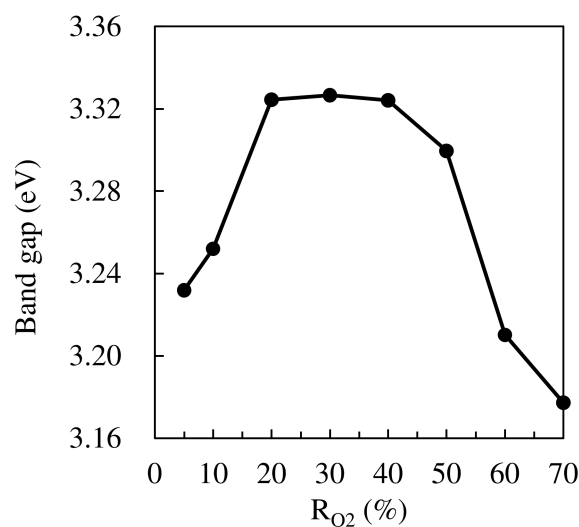


Figure 4. Band gaps of TiO₂ thin.

3.3. SEM Images

The surface morphologies were investigated by FE-SEM measurements (Figure 5). The average diameters were 23 and 25 nm for the film deposited under $R_{O_2} = 5\%$ and 50%, respectively. Thus, it is suggested that the morphology does not change at the value of $R_{O_2} = 50\%$.

The thickness of TiO₂ films was measured by the cross-sectional FE-SEM images and the interference of transmitted light. Figure 6 shows that the films gradually became thinner as the R_{O_2} increased, indicating that the growth rate of the films became slower with increasing R_{O_2} . At high R_{O_2} (low Ar gas ratio), the plasma generation generally becomes more difficult because Ar can more easily be dissociated than O₂; the dissociation energy of the Ar was about 15.76 eV, and O₂ was approximately 48.77 eV [19]. Therefore, a possible explanation of the thinner film at high R_{O_2} is that the plasma sputtering rate becomes less intensive.

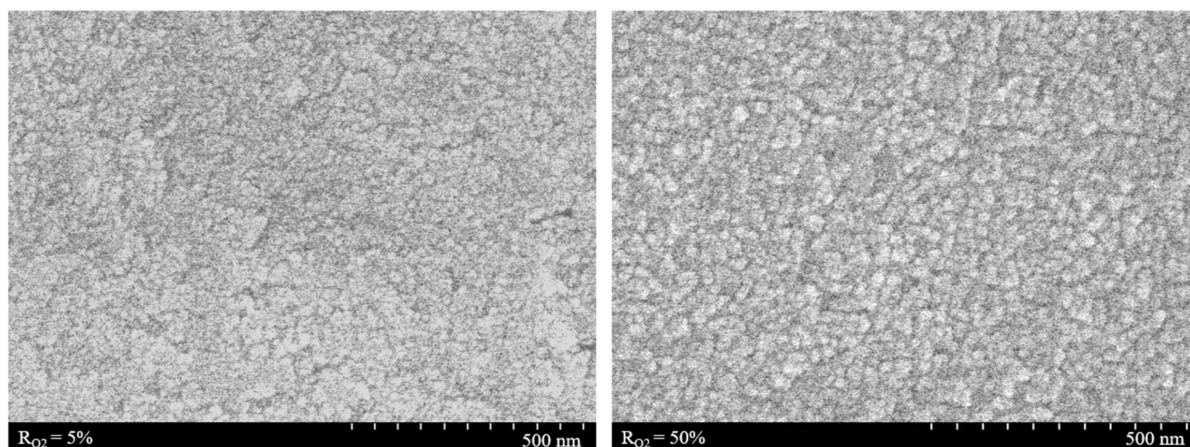


Figure 5. Surface morphologies of TiO₂ thin films prepared at R_{O₂} = 5% (left) and 50% (right).

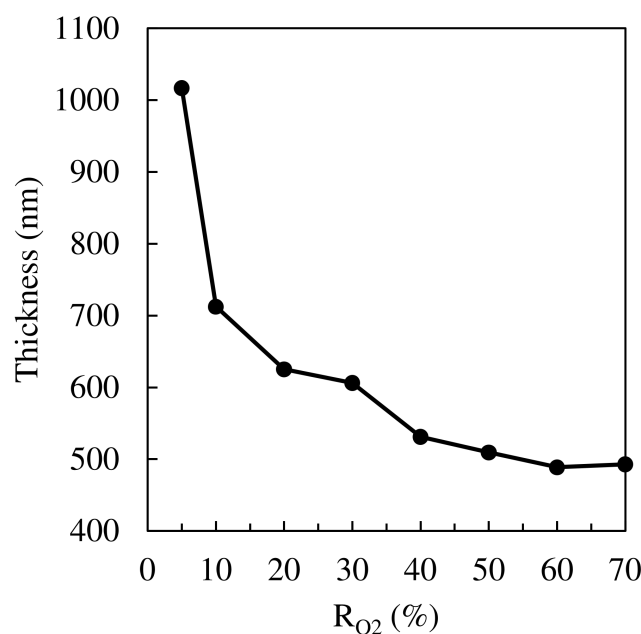


Figure 6. Thickness of TiO₂ thin films.

3.4. XPS Measurements

The XPS measurements were performed to examine the chemical states of Ti in proximity to surfaces of TiO₂ thin films. Figure 7 shows the high-resolution narrow scan of XPS spectra around the Ti 2p^{3/2} spin orbital. The main peak (458.0 eV) is ascribed to the Ti⁴⁺ state, and the shoulder peak in the lower binding energy region (456.5 eV) is assigned to the Ti³⁺ state. The ratio of Ti³⁺ to Ti⁴⁺ corresponds to the oxygen vacancy ratio in TiO₂ thin films because Ti³⁺ is generated when Ti⁴⁺ in TiO₂ is reduced and releases oxygen [25]. Figure 8 summarizes the Ti³⁺ ratio changes as a function of R_{O₂}. It is noteworthy that the TiO₂ film deposited under the most oxygen-rich condition (R_{O₂} = 70%) has the highest amount of oxygen vacancies.

3.5. Photocatalytic Activity

Figure 9a shows the photocatalytic activity of the TiO₂ thin films for MO degradation. As indicated by the control test (blank concentration) fluctuation, the error in the concentration measurement is at least 4.3%. To evaluate the photocatalytic activities, we employed the MO concentrations at 80 min (Figure 9b), where the decomposed MO amount is significant even considering the measurement error. We then found similar behavior in the degradation rate as well as other properties: that is, with the R_{O₂} increase, the degradation

rate is decreased until $R_{O_2} = 30\%$, while the rate is increased over $R_{O_2} = 40\%$. The TiO_2 film synthesized under $R_{O_2} = 70\%$ showed the highest photocatalytic activity. The correlation between catalytic activity and the other properties will be discussed in the next section.

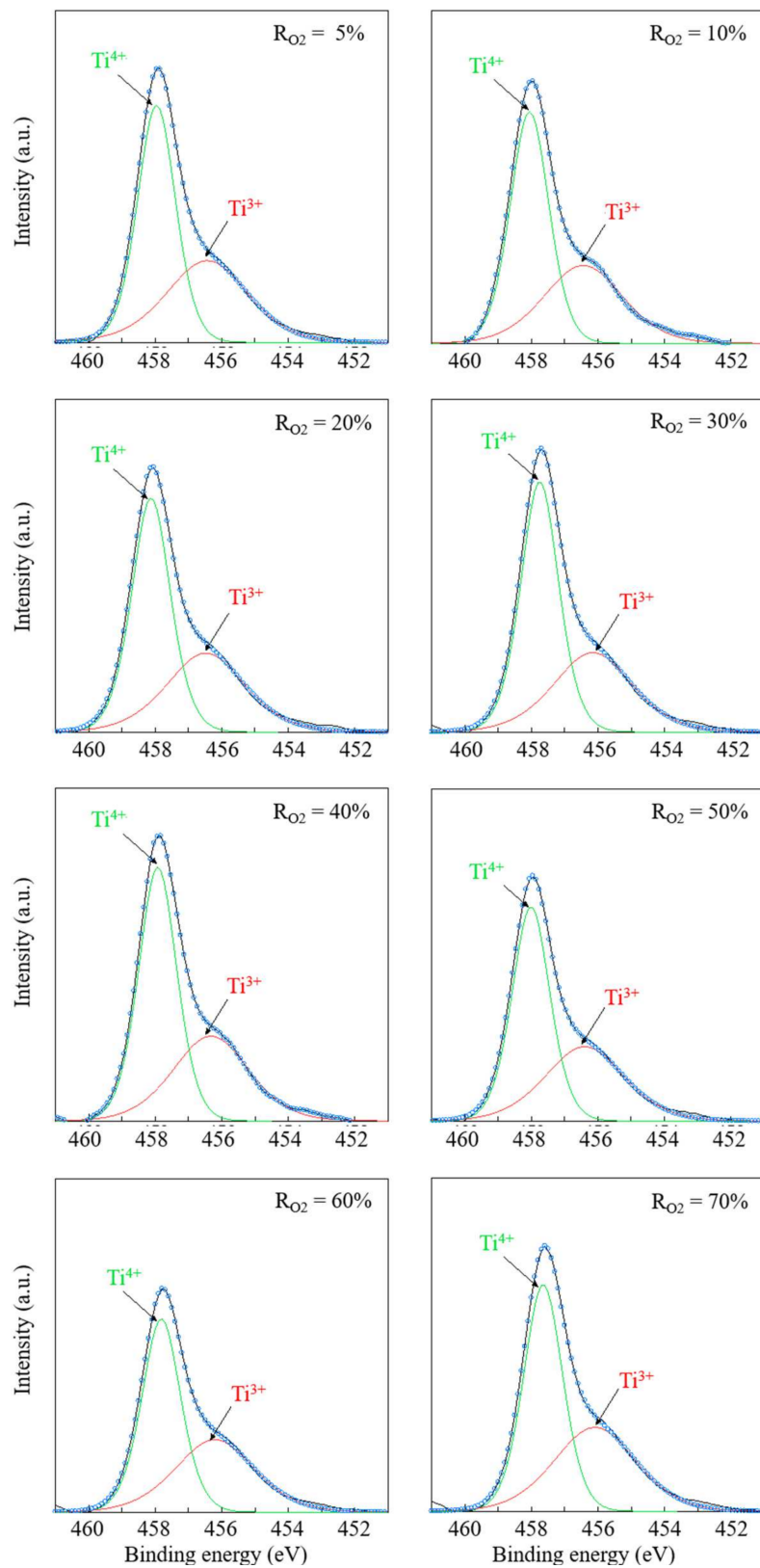


Figure 7. XPS results for the binding energy of Ti^{3+} versus Ti^{4+} in TiO_2 thin films.

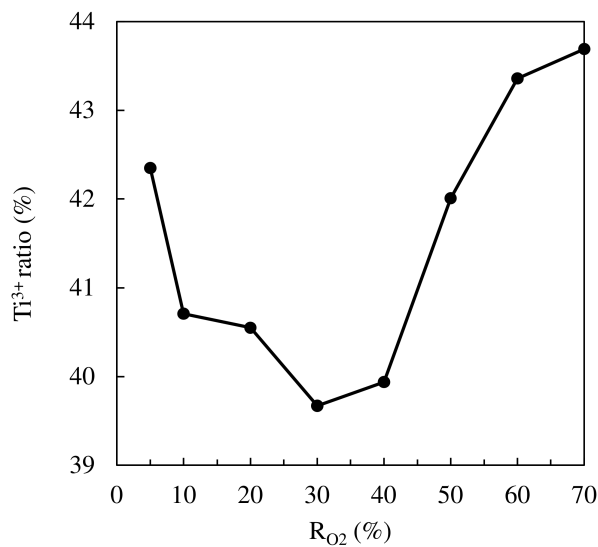


Figure 8. The ratio of Ti³⁺ to Ti⁴⁺ in TiO₂ thin films.

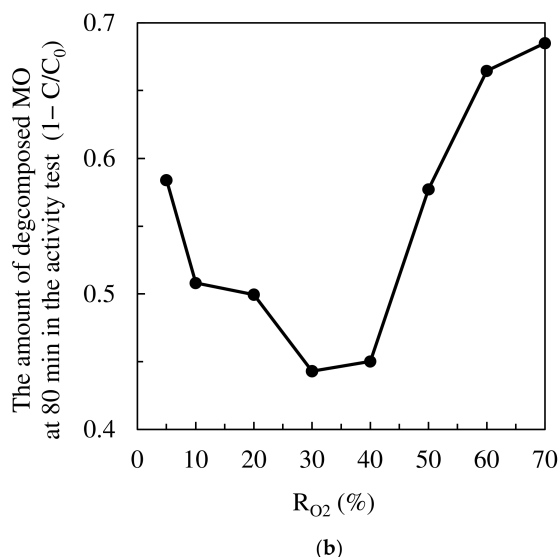
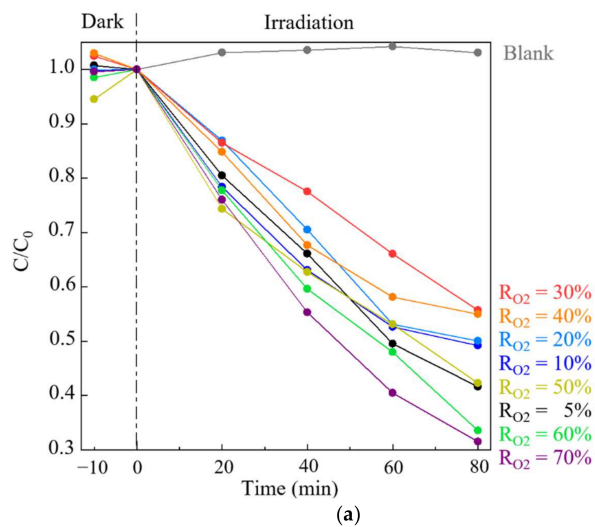


Figure 9. The catalytic activity of TiO₂ thin films for MO degradation. C₀ and C are the concentrations of MO solution at the initial and at each minute, respectively. (a) The concentration changes over time and (b) the amount of decomposed MO at 80 min during the activity test (1 - C/C₀).

To check whether Ti^{3+} reacts with MO to become Ti^{4+} , we estimated the amount of Ti^{3+} using the thickness of the films and compared them with the amount of decomposed MO after 80 min irradiation. The amount of decomposed MO is about six orders of magnitude higher than that of Ti^{3+} in TiO_2 thin film. Therefore, the contribution of Ti^{3+} to the decomposition of MO, via sacrificing itself to become Ti^{4+} , was negligible.

4. Discussion

4.1. Plausible Explanation of a Less Oxidized State Induced under the Oxygen-Rich Condition

In this section, we suggest a possible explanation for why the less oxidized state appeared in the TiO_2 thin films prepared under the oxygen-rich condition, $R_{\text{O}_2} = 40\text{--}70\%$. According to a previous study [26], oxygen-rich conditions facilitate the nucleation of the rutile structure. Similar behavior regarding crystal structure changes was also reported in another study; as R_{O_2} was increased, the rutile structure disappeared first and appeared again when the synthesis condition became oxygen-rich, and they discussed these phenomena from reactive mechanics in the deposition [27,28]. Hence, the increase in the rutile structure in the oxygen-rich condition is reasonable. Furthermore, the ab initio calculation indicates that the rutile structure with (110) facets favors the oxygen vacancies on the surface, rather than the anatase structure with its most stable (101) facet, since their formation energy at the rutile (110) surface is smaller than that at the subsurface and much smaller than that in bulk rutile [29,30], which is consistent with our XPS results. Therefore, a higher concentration of oxygen vacancies is mainly observed due to an increased amount of the rutile structure, which is produced under oxygen-rich conditions.

4.2. Origin of High Photocatalytic Activity

The photocatalytic activity is generally related to the crystal structure [31–33], band gap [4], surface morphology [3], and the amount of oxygen vacancy [34–36]. However, the FE-SEM images show that the surface morphology did not change when comparing the samples prepared under $R_{\text{O}_2} = 5\%$ and 50% . Hence, the surface morphology is unlikely related to the change in the degradation rate. The other three parameters (crystal structure, band gap, and the amount of oxygen vacancy) are then considered to further examine the origin of enhanced photocatalytic activity.

Figure 10 shows the relation between the photocatalytic activity and the band gap (a) or the Ti^{3+} ratio (b). Based on the XRD patterns, the TiO_2 thin films synthesized under $R_{\text{O}_2} = 20\text{--}30\%$ have only the anatase structure, whereas the samples prepared under $R_{\text{O}_2} = 5\text{--}10$ and $40\text{--}70\%$ were composites of the anatase and the rutile structure. Although the reference [27] indicated that only one of the two structures was formed dominantly at $R_{\text{O}_2} = 70\%$, our sample showed both peaks are distinguished in XRD results, which seems derived from some other conditions. Generally, the anatase structure is more active than the rutile structure [37]. However, rutile/anatase composites could show higher activity than the anatase structure alone [31–33], because the composite interface (heterojunction) may disturb the recombination of electrons and holes. In addition, the narrow band gap is preferable for absorbing more light, though a weak correlation between band gap and decomposition rate is seen, as shown in Figure 10a. Therefore, higher activity is likely influenced by the existence of composites.

Oxygen vacancies are also involved in promoting charge separation and disturbing the electron–hole recombination process, resulting in high photocatalytic activity [34–36]. Then, a relatively large amount of oxygen vacancy in the TiO_2 samples could be responsible for high photocatalytic activity. Although the pre-sputtering in XPS measurement removes the outermost surface layer (~ 0.2 nm) and detects the chemical composition in the subsurface, the oxygen vacancies in the subsurface layer could have a strong potential to enhance the photocatalytic activity [38]. Thus, the seemingly strong correlation shown in Figure 10b can be significant and explained in a consistent manner. It is noted that, though the discussed Ti^{3+} ratio may not be exactly the same with the as-sputtered surface due to some reduction of Ti^{4+} to Ti^{3+} via Ar ion etching, the difference of the reduction among samples could be

negligible, and our XPS results on the tendency of Ti^{3+} ratio are inconsistent with the change in XRD patterns, band gap, and photocatalytic activity. It is then plausible that our XPS results are correlated to the oxygen vacancies in the original states. Therefore, the excellent correlation between Ti^{3+} ratio and degradation rate, as shown in Figure 10b, strongly suggests that the oxygen vacancies have a solid potential to enhance photocatalytic activity.

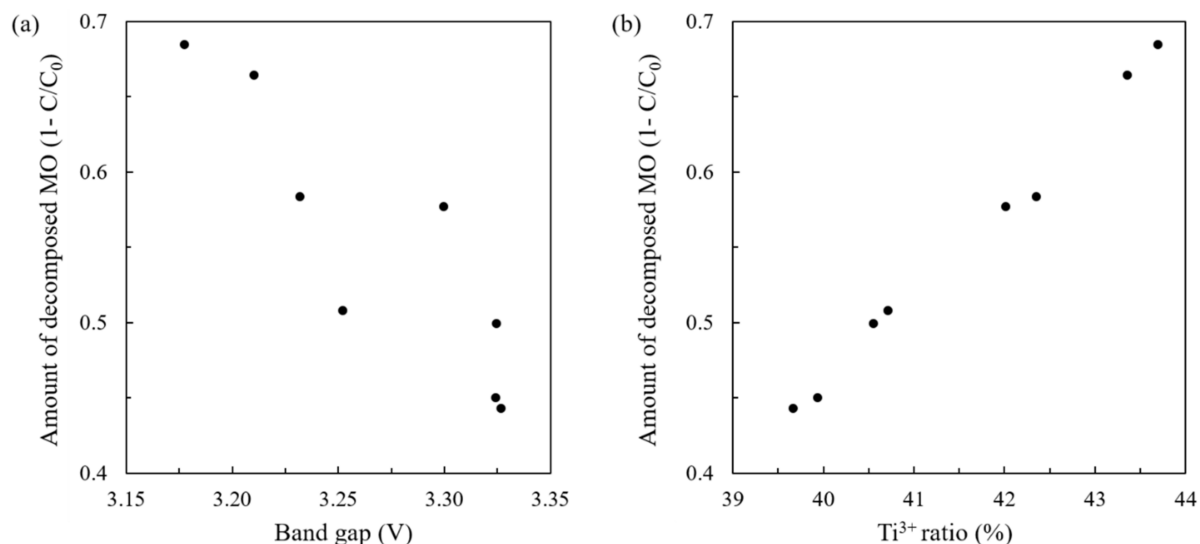


Figure 10. The relationship between the amount of decomposed MO at 80 min during the activity test ($1 - C/C_0$) and (a) Ti^{3+} ratio and (b) band gap. C_0 and C are the concentration of MO solution at the initial and at each minute, respectively.

Hence, we can conclude that a large amount of oxygen vacancy, the narrower band gap, and the existence of rutile/anatase composites play an essential role in enhancing photocatalytic activity. It could be easy to prepare the thin films using reactive RF sputtering under the less oxygen flow condition to attain these three factors in the satisfactory range. However, this study shows that it is also possible or preferable in higher oxygen flow conditions.

5. Conclusions

The TiO_2 thin films were prepared via reactive RF sputtering under various flow rates of oxygen and argon gas. We observed the highest photocatalytic activity for the films prepared under the most oxygen-enriched condition among the prepared samples, 70%. The origin of the enhanced activity is attributed to the composite of anatase/rutile structure and the increased oxygen vacancy despite the oxygen-rich sputtering condition. The reason why a less oxidized state appeared under the oxygen-enriched condition is as follows: the rutile structure prefers to grow under oxygen-rich conditions at around room temperature and tends to generate a higher concentration of oxygen vacancies. Therefore, this research presents the insight that the less oxidized state of TiO_2 films can be prepared even in an oxygen-rich condition. The conditions could be useful for preparing highly photoactive TiO_2 thin films.

Supplementary Materials: The following supporting information can be downloaded at: <https://www.mdpi.com/article/10.3390/photochem2010011/s1>, Figure S1: Spectral irradiance of the Xenon lamp; Table S1: The comparison of sputtering condition in several pieces of literature; Table S2: The crystallite size of TiO_2 thin films estimated via Scherrer's equation based on anatase (101) plane.

Author Contributions: Writing—original draft: T.O.; Formal analysis, Writing—review & editing, Validation: Y.Z.; K.N.I.; Data curation: T.O.; Y.Z.; H.O.; Investigation: T.O.; Y.Z.; All authors have read and agreed to the published version of the manuscript.

Funding: This research received no external funding.

Institutional Review Board Statement: Not applicable.

Informed Consent Statement: Not applicable.

Conflicts of Interest: The authors declare no conflict of interest.

References

1. Patel, N.; Fernandes, R.; Guella, G.; Kale, A.; Miotello, A.; Patton, B.; Zanchetta, C. Structured and nanoparticle assembled Co–B thin films prepared by pulsed laser deposition: A very efficient catalyst for hydrogen production. *J. Phys. Chem. C* **2008**, *112*, 6968–6976. [[CrossRef](#)]
2. Anpo, M.; Takeuchi, M. The design and development of highly reactive titanium oxide photocatalysts operating under visible light irradiation. *J. Catal.* **2003**, *216*, 505–516. [[CrossRef](#)]
3. Yu, J.G.; Zhao, X.J.; Zhao, Q.N. Effect of surface structure on photocatalytic activity of TiO₂ thin films prepared by sol-gel method. *Thin Solid Films* **2000**, *379*, 7–14. [[CrossRef](#)]
4. Hoffmann, M.R.; Martin, S.T.; Choi, W.Y.; Bahnemann, D.W. Environmental applications of semiconductor photocatalysis. *Chem. Rev.* **1995**, *95*, 69–96. [[CrossRef](#)]
5. Carp, O.; Huisman, C.L.; Reller, A. Photoinduced reactivity of titanium dioxide. *Prog. Solid State Chem.* **2004**, *32*, 33–177. [[CrossRef](#)]
6. Hieu, V.Q.; Lam, T.C.; Khan, A.; Thi Vo, T.-T.; Nguyen, T.-Q.; Doan, V.D.; Tran, D.L.; Le, V.T.; Tran, V.A. TiO₂/Ti₃C₂/g-C₃N₄ ternary heterojunction for photocatalytic hydrogen evolution. *Chemosphere* **2021**, *285*, 131429. [[CrossRef](#)] [[PubMed](#)]
7. Hieu, V.Q.; Phung, T.K.; Nguyen, T.-Q.; Khan, A.; Doan, V.D.; Tran, V.A.; Le, V.T. Photocatalytic degradation of methyl orange dye by Ti₃C₂–TiO₂ heterojunction under solar light. *Chemosphere* **2021**, *276*, 130154. [[CrossRef](#)] [[PubMed](#)]
8. Chung, C.K.; Liao, M.W.; Lai, C.W. Effects of oxygen flow ratios and annealing temperatures on raman and photoluminescence of titanium oxide thin films deposited by reactive magnetron sputtering. *Thin Solid Films* **2009**, *518*, 1415–1418. [[CrossRef](#)]
9. Pomoni, K.; Vomvas, A.; Trapalis, C. Electrical conductivity and photoconductivity studies of TiO₂ sol–gel thin films and the effect of N-doping. *J. Non-Cryst. Solids* **2008**, *354*, 4448–4457. [[CrossRef](#)]
10. Natarajan, C.; Fukunaga, N.; Nogami, G. Titanium dioxide thin film deposited by spray pyrolysis of aqueous solution. *Thin Solid Films* **1998**, *322*, 6–8. [[CrossRef](#)]
11. Terashima, M.; Inoue, N.; Kashiwabara, S.; Fujimoto, R. Photocatalytic TiO₂ thin-films deposited by pulsed laser deposition technique. *IEEJ Trans. Fundam. Mater.* **2001**, *121*, 59–64. [[CrossRef](#)]
12. Sun, L.; Hou, P. Spectroscopic ellipsometry study on e-beam deposited titanium dioxide films. *Thin Solid Films* **2004**, *455–456*, 52–529. [[CrossRef](#)]
13. Sun, H.; Wang, C.; Pang, S.; Li, X.; Tao, Y.; Tang, H.; Liu, M. Photocatalytic TiO₂ films prepared by chemical vapor deposition at atmosphere pressure. *J. Non-Cryst. Solids* **2008**, *354*, 1440–1443. [[CrossRef](#)]
14. Boukrouh, S.; Bensaha, R.; Bourgeois, S.; Finot, E.; Marco de Lucas, M.C. Reactive direct current magnetron sputtered TiO₂ thin films with amorphous to crystalline structures. *Thin Solid Films* **2008**, *516*, 6353–6358. [[CrossRef](#)]
15. Chiu, S.-M.; Chen, Z.-S.; Yang, K.-Y.; Hsu, Y.-L.; Gan, D. Photocatalytic activity of doped TiO₂ coatings prepared by sputtering deposition. *J. Mater. Process. Technol.* **2007**, *192–193*, 60–67. [[CrossRef](#)]
16. Wang, Y.-H.; Rahman, K.H.; Wu, C.-C.; Chen, K.-C. A review on the pathways of the improved structural characteristics and photocatalytic performance of titanium dioxide (TiO₂) thin films fabricated by the magnetron-sputtering technique. *Catalysts* **2020**, *10*, 598. [[CrossRef](#)]
17. Zhang, W.; Li, Y.; Zhu, S.; Wang, F. Influence of argon flow rate on TiO₂ photocatalyst film deposited by dc reactive magnetron sputtering. *Surf. Coat. Technol.* **2004**, *182*, 192–198. [[CrossRef](#)]
18. Huang, C.H.; Tsao, C.C.; Hsu, C.Y. Study on the photocatalytic activities of TiO₂ films prepared by reactive RF sputtering. *Ceram. Int.* **2011**, *37*, 2781–2788. [[CrossRef](#)]
19. Chiou, A.H.; Kuo, C.G.; Huang, C.H.; Wu, W.F.; Chou, C.P.; Hsu, C.Y. Influence of oxygen flow rate on photocatalytic TiO₂ films deposited by RF magnetron sputtering. *J. Mater. Sci. Mater. Electron.* **2011**, *23*, 589–594. [[CrossRef](#)]
20. Machda, F.; Ogawa, T.; Okumura, H.; Ishihara, K.N. Damp heat durability of Al-doped ZnO transparent electrodes with different crystal growth orientations. *ECS J. Solid State Sci. Technol.* **2019**, *8*, Q240–Q244. [[CrossRef](#)]
21. Wang, L.-Q.; Baer, D.R.; Engelhard, M.H. Creation of variable concentrations of defects on TiO₂(110) using low-density electron beams. *Surf. Sci.* **1994**, *320*, 295–306. [[CrossRef](#)]
22. Yu, J.-G.; Yu, H.-G.; Cheng, B.; Zhao, X.-J.; Yu, J.C.; Ho, W.-K. The effect of calcination temperature on the surface microstructure and photocatalytic activity of TiO₂ thin films prepared by liquid phase deposition. *J. Phys. Chem. B* **2003**, *107*, 13871–13879. [[CrossRef](#)]
23. Paul, A.; John, J.C.; Augustine, S.; Sebastian, T.; Joy, A.; Joy, J.; Maria Michael, T. Comparison of photocatalytic efficiency of TiO₂ and In₂S₃ thin films under UV and visible light irradiance. *Adv. Mater. Lett.* **2020**, *11*, 1–7. [[CrossRef](#)]
24. Bharti, B.; Kumar, S.; Lee, H.N.; Kumar, R. Formation of oxygen vacancies and Ti³⁺ state in TiO₂ thin film and enhanced optical properties by air plasma treatment. *Sci. Rep.* **2016**, *6*, 32355. [[CrossRef](#)]
25. Farfan-Arribas, E.; Madix, R.J. Role of defects in the adsorption of aliphatic alcohols on the TiO₂(110) surface. *J. Phys. Chem. B* **2002**, *106*, 10680–10692. [[CrossRef](#)]

26. Löbl, P.; Huppertz, M.; Mergel, D. Nucleation and growth in TiO₂ films prepared by sputtering and evaporation. *Thin Solid Films* **1994**, *251*, 72–79. [[CrossRef](#)]
27. Zeman, P.; Takabayashi, S. Effect of total and oxygen partial pressures on structure of photocatalytic TiO₂ films sputtered on unheated substrate. *Surf. Coat. Technol.* **2002**, *153*, 93–99. [[CrossRef](#)]
28. Schiller, S.; Beister, G.; Sieber, W.; Schirmer, G.; Hacker, E. Influence of deposition parameters on the optical and structural properties of TiO₂ films produced by reactive D.C. Plasmatron sputtering. *Thin Solid Films* **1981**, *83*, 239–245. [[CrossRef](#)]
29. Cheng, H.; Selloni, A. Surface and subsurface oxygen vacancies in anatase TiO₂ and differences with rutile. *Phys. Rev. B* **2009**, *79*, 092101 .
30. Li, H.; Guo, Y.; Robertson, J. Calculation of TiO₂ surface and subsurface oxygen vacancy by the screened exchange functional. *J. Phys. Chem. C* **2015**, *119*, 18160–18166. [[CrossRef](#)]
31. Ohno, T.; Tokieda, K.; Higashida, S.; Matsumura, M. Synergism between rutile and anatase TiO₂ particles in photocatalytic oxidation of naphthalene. *Appl. Catal. A* **2003**, *244*, 383–391. [[CrossRef](#)]
32. Kho, Y.K.; Iwase, A.; Teoh, W.Y.; Mädler, L.; Kudo, A.; Amal, R. Photocatalytic H₂ evolution over TiO₂ nanoparticles. The synergistic effect of anatase and rutile. *J. Phys. Chem. C* **2010**, *114*, 2821–2829. [[CrossRef](#)]
33. Su, R.; Bechstein, R.; Sør, L.; Vang, R.T.; Sillassen, M.; Esbjörnsson, B.; Palmqvist, A.; Besenbacher, F. How the anatase-to-rutile ratio influences the photoreactivity of TiO₂. *J. Phys. Chem. C* **2011**, *115*, 24287–24292. [[CrossRef](#)]
34. Nowotny, M.K.; Sheppard, L.R.; Bak, T.; Nowotny, J. Defect chemistry of titanium dioxide. Application of defect engineering in processing of TiO₂-based photocatalysts. *J. Phys. Chem. C* **2008**, *112*, 5275–5300. [[CrossRef](#)]
35. Wang, J.; Liu, P.; Fu, X.; Li, Z.; Han, W.; Wang, X. Relationship between oxygen defects and the photocatalytic property of ZnO nanocrystals in Nafion membranes. *Langmuir* **2009**, *25*, 1218–1223. [[CrossRef](#)]
36. Pan, X.; Yang, M.Q.; Fu, X.; Zhang, N.; Xu, Y.J. Defective TiO₂ with oxygen vacancies: Synthesis, properties and photocatalytic applications. *Nanoscale* **2013**, *5*, 3601–3614. [[CrossRef](#)]
37. Sclafani, A.; Herrmann, J.M. Comparison of the photoelectronic and photocatalytic activities of various anatase and rutile forms of titania in pure liquid organic phases and in aqueous solutions. *J. Phys. Chem.* **1996**, *100*, 13655–13661. [[CrossRef](#)]
38. Lee, S.-H.; Yamasue, E.; Ishihara, K.N.; Okumura, H. Photocatalysis and surface doping states of N-doped TiO_x films prepared by reactive sputtering with dry air. *Appl. Catal. B* **2010**, *93*, 217–226. [[CrossRef](#)]